Laser and Particle Beams (2002), *20*, 87–92. Printed in the USA.

DOI: 10.1017.S0263034602201123

Laser-induced tension to measure the ultimate strength of metals related to the equation of state

SHALOM ELIEZER,[1] ELLA MOSHE,[1] AND DAN ELIEZER[2]
[1]Plasma Physics Department, Soreq NRC, Yavne 81800, Israel
[2]Department of Materials Engineering, Ben-Gurion University, Beer-Sheva, Israel

(RECEIVED 12 June 2001; ACCEPTED 8 October 2001)

Abstract

The approach to the ultimate strength of metals is determined experimentally. The strength of the materials and the strain rate were determined from the free surface velocity time history, which was measured with an optically recording velocity interferometer system. The dynamic strength was measured at strain rates in the domain of $5 \cdot 10^6$ to $5 \cdot 10^8$ s^{-1}. The necessary tension to break the metal (spall) and the very high strain rates were achieved using high-powered lasers in nanosecond and picosecond regimes. The measurements at strain rates larger than 10^8 s^{-1} were achieved for the first time. The ultimate strength of metals was calculated using a realistic wide-range equation of state. Our experiments indicate that under very fast tension processes, the dynamic strength of materials is determined not by the macroscopic defects but by atomic quantum mechanical processes described by the equation of state of the material. The rate of the process is described by the strain rate, and at strain rates higher than $5 \cdot 10^7$ s^{-1}, the atomic forces are dominating the dynamic strength of materials.

Keywords: Dynamic fracture; Equation of state; Shock wave; Spall; Strain rate

1. INTRODUCTION

A spall is a dynamic fracture in the material caused by an intense impulsive load. It is characterized by a planar separation of the sample, parallel to a stress wave front (Fig. 1).

The strain which has been formed at the spall area is defined by $\epsilon = \Delta l/l$ where Δl is the difference between the final and the original lengths of the target in one dimension and l is the original length. The strain rate is given by $\dot{\epsilon} = d\epsilon/dt$.

To create high strain rates, high-power short-pulse lasers have to be used. The high-power laser–target interaction produced a propagating shock wave in the material (Fig. 2a).

When the shock wave is reflected from the rear surface of a metallic sample, the compressed material expands freely and a rarefaction wave returns toward the front surface. The expansion leads to tension in the material and to a deceleration of the rear surface. Meanwhile, at the end of the laser pulse, a second rarefaction wave propagates from the front surface as the pressure loading starts to fall off. The superposition of these two rarefaction waves induces a dynamic tensile stress (Fig. 2b).

If the magnitude and duration of this tensile stress exceeds the material's strength, spallation occurs in a plane parallel to the rear surface (Grady, 1988; Bushman *et al.*, 1993*a*, 1993*b*; Grady & Kipp, 1993). The spall thickness is the distance between the spall plane and the rear surface. The spall strength of the material is determined from the measurement of the free surface velocity time history.

2. EXPERIMENTS

The experiments were performed at the high-power laser laboratory in Soreq. Figure 3 is a schematic description of the experimental setup.

The diagnostic interferometric system called ORVIS (optically recording velocity interferometer system; Bloomquist & Sheffield, 1983; Moshe *et al.*, 1996) consists on a laser focused on the rear surface aligned accurately against the spot of the main laser beam. The light reflected from the moving free surface undergoes a Doppler shift proportional to the velocity of the free surface. The light is collected, collimated, and reflected into a Michelson interferometer. A beam splitter divides the beam into two nonequal legs. An

Address correspondence and reprint requests to: Shalom Eliezer, Plasma Physics Department, Soreq NRC, Yavne 81800, Israel. E-mail: eliezer@soreq.gov.il

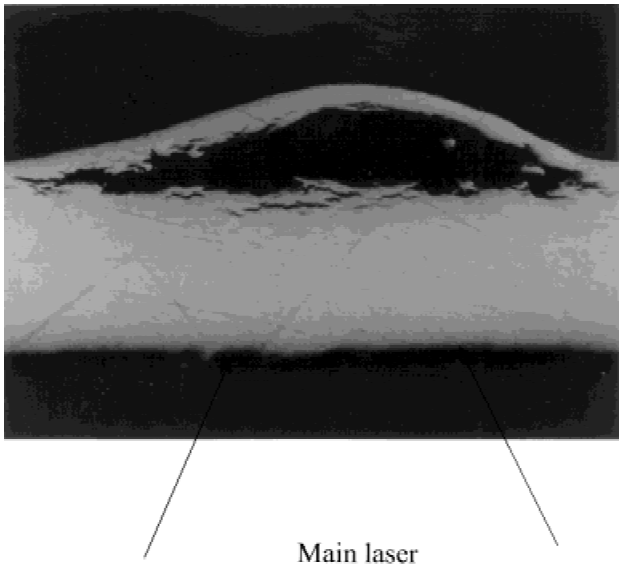

Fig. 1. Crossection in an Al 6061 target after the spall creation. The thickness of the target is 100 μm.

Etalon is placed in the route of one of the legs. The two beams are back reflected and than recombined. The recombination of the two beams produces an interference pattern of parallel fringes. These fringes are generated from light, which was reflected from the target at two different times. Therefore when the target is accelerated (or decelerated) the fringes are shifted. The interference pattern is imaged by a cylindrical lens to a set of bright points on the entrance slit of a streak camera. The interference pattern is analyzed with an image processing system, including a cooled charged-coupled device camera, a frame grabber, and a PC.

This diagnostic technique provides an accurate, continuous measurement of the surface velocity, which has the advantage of not interfering with the motion of the shocked target. The spall strength, the strain rate, and the pressure can be inferred from the profile of the velocity in time. The velocity history of the moving rear surface, $u(t)$, was determined from the displacement of the interference pattern. The velocity of the moving surface is related to the vertical position $y(t)$ of the interference pattern as a function of time (Barker & Schuler, 1974; Bloomquist & Sheffield, 1983; Baumung & Singer, 1995):

$$u(t) = u_0 \frac{y(t)}{d}, \tag{1}$$

where d is the perpendicular distance between two adjacent lines before movement and u_0 is the fringe constant and is given by

$$u_0 = \frac{\lambda_0}{2\tau} \cdot \frac{2}{(1+\delta)}, \tag{2}$$

λ_0 is the diagnostic laser wavelength, δ is a correction of the Etalon index of refraction due to change of wavelength during the experiment. n_0 is the index of refraction of the Etalon material for λ_0 and c is the light velocity. τ is a function of the Etalon length, h_e:

$$\tau = \frac{2h_e}{c}\left(n_0 - \frac{1}{n_0}\right). \tag{3}$$

The wide range of strain rates and the different materials required the development of three different experimental systems, which were designed for different purposes (Table 1).

The first system is based on a nanosecond laser for causing the shock wave and a 1.5-W continuous wave argon laser for the diagnostic system. For this system, we used targets with good reflectance—aluminum, copper, zinc, and tin. The strain rate here was in the range of 10^7 s^{-1}. To check the assumption that material dislocations were reducing the spall strength, we used a material that has no dislocations—the amorphous alloy $Fe_{80}B_{11}S_9$. Because this material has very low reflectivity we had to design a diagnostic source that supplies much more light so that we can follow the history of the rear surface velocity. This was the second system. This diagnostic system supplies 300 W compared to 1.5 W in the first system.

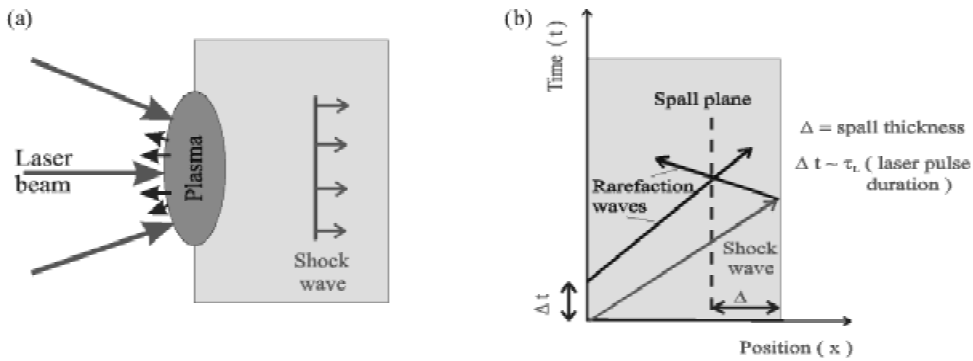

Fig. 2. Laser-induced damage: (a) Shock wave creation. (b) Spall creation.

https://doi.org/10.1017/S0263034602201123 Published online by Cambridge University Press

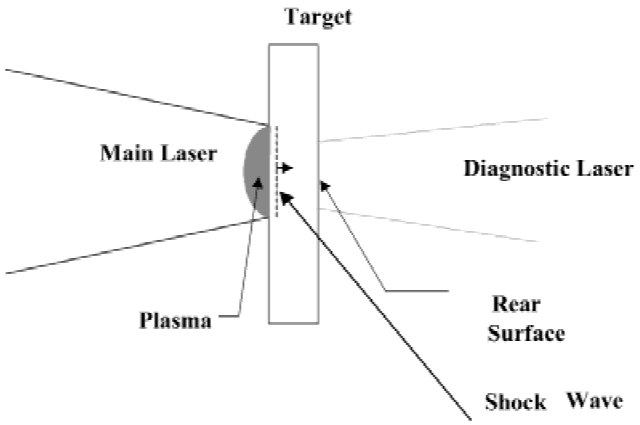

Fig. 3. Schematic description of the experimental setup.

To approach the strength corresponding to the equation of state, we changed to a picosecond laser to create the pressure on the target. This is the third experimental system. With this system, we actually got to strain rates of $3 \cdot 10^8\ s^{-1}$. Because the phenomenon is extremely short in this regime, we used the nanosecond laser for diagnostics at a level of 10^5 W.

Figure 4a is a typical fringe pattern representing the free surface velocity history that was obtained with the ORVIS. Figure 4b shows the experimental data, that is, the rear surface velocity as a function of time, as derived from Figure 4a.

In this experiment, a 7-ns, 36-J laser pulse focused to a 600-μm diameter spot hits the front of a 50-μm-thick zinc target. Time is increasing from left to right. The full time scale of this figure is 68 ns and the distance between two fringes (the fringe constant) is 0.301 km/s. The fringes are parallel to the time axis until the rear surface undergoes acceleration, where the fringe pattern starts shifting.

In the experiments reported, the spot size of the laser beam generating the shock wave was more than one order of magnitude larger than the foil's thickness, resulting in a one-dimensional geometry of the waves propagating within the target.

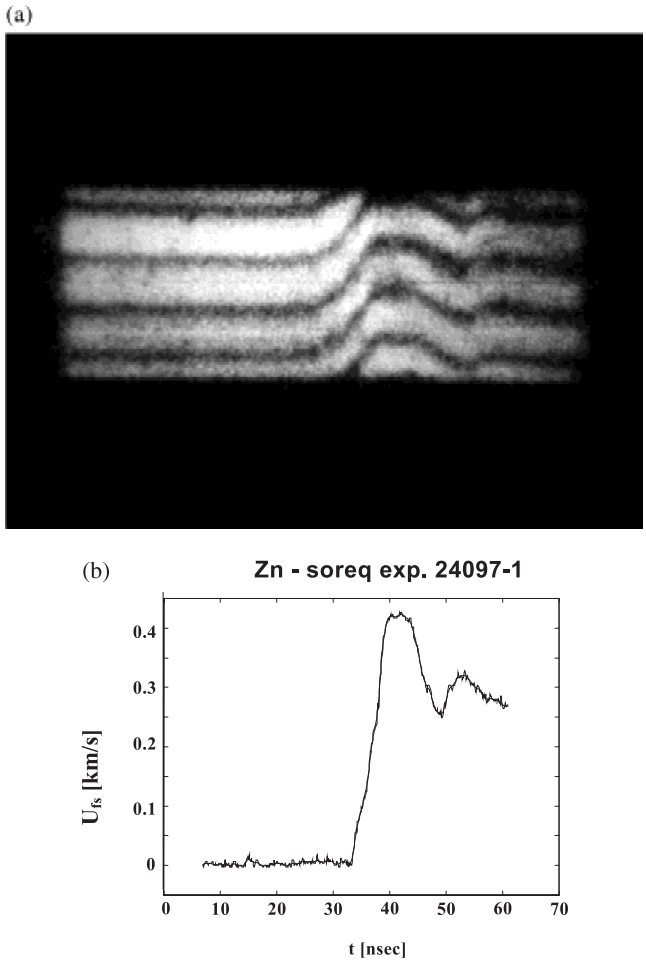

Fig. 4. (a) Interference pattern in an experiment with zinc (laser shot no. 24097-1); horizontal axis: 68 ns (full scale); vertical axis: fringe constant: 0.301 km/s. (b) The free surface velocity as a function of time.

3. DISCUSSION

The first shift is the arrival of the first shock wave to the rear surface. Upon arrival of the shock wave to the rear surface, a rarefaction wave is returning into the material, accelerating the rear surface to approximately double the velocity of the particles behind the shock front. The material is carried into tension and the rear surface is decelerated. When the tension (negative pressure) is high enough, spalling occurs within the material, leading to a second shock wave which arrives at the rear surface, which starts accelerating.

The spall strength was determined from the measured time dependence of the free surface velocity (Kanel *et al.*,

Table 1. *The three different experimental systems*

	The laser creating the shock wave			The diagnostic laser in the ORVIS system		
	Wavelength	Irradiance	Pulse length	Wavelength	Irradiance	Pulse length
A	1.06 μm	10^{13}–10^{11} W/cm^2	7–2 ns	0.514 μm (Ar)	1.5 W	continuous
B	1.06 μm	10^{13}–10^{11} W/cm^2	7–2 ns	0.532 μm (SHG Nd:YAG)	300 W	100 ns
C	1.06 μm	10^{13}–10^{11} W/cm^2	20 ps or 100 ps	0.532 μm (SHG Nd:YAG)	10^5 W	10 ns

SHG = Second harmonic generation.

https://doi.org/10.1017/S0263034602201123 Published online by Cambridge University Press

1993, 1996*b*; Dekel *et al.*, 1998). $P_{spall} = \rho_0 c_0 (u_{max} - u_{min})/2$, c_0 is the sound velocity, ρ_0 is the initial density of the target, u_{max} is the peak velocity of the free surface, and u_{min} is the first minimum of the free-surface profile. The strain rate was calculated by $\dot{\epsilon} = (\Delta u/\Delta t)/(2c_0)$, Δu is the velocity difference between the first maximum and the first minimum in the free surface velocity profile and Δt is the difference between the corresponding times.

The shock pressure near the rear surface of the target was estimated from the peak velocity of the free surface, u_{max}. The particle velocity in the shocked material is given by $u_p = u_{max}/2$. The shock velocity and the pressure were determined from Hugoniot relations and the equation of state (EOS). The EOS yields the known relation $u_s = c_0 + a \cdot u_p$, where u_s is the shock velocity and a is a constant. The pressure is given by the Hugoniot relation $P = \rho_0 u_s u_p$.

To check the assumption that material dislocations reduce the spall strength at low strain rates and do not affect it at high strain rates (Eliaz *et al.*, 2000), we used a material that has no dislocations—the amorphous alloy $Fe_{80}B_{11}S_9$. The dynamic strength of $Fe_{80}B_{11}S_9$ was measured in two cases: first, when it was charged with hydrogen and, second, without hydrogen charging. The morphology of the spall region was analyzed using a scanning electron microscope. Microscopically, one sees that the charged material was full of bubbles and cracks joining the bubbles, while the uncharged material was almost homogeneous and clean of faults. In addition, we measured the spall strength of pure crystalline iron. We found that at high strain rates, the two amorphous materials (charged and uncharged with hydrogen) have the same strength. The strength of the crystalline iron was also similar at high strain rates. This shows that at high strain rates, the cracks do not have time to move and coalesce and the material strength is not affected by the faults. The static strength of crystalline Fe is much smaller than the dynamic strength, but the static strength of the amorphous alloy is similar to its dynamic strength. In spite of the fact that the initial conditions of "damages" in the charged amorphous alloy are significantly different from the uncharged material, the dynamic results are the same. It means that at high strain rates, the strength is determined mainly by the interatomic forces and not by the initial damages in the material.

The ultimate spall strength, that is, the stress needed to separate the material along a plane surface instantaneously, is determined theoretically from the EOS. The EOS are a thermodynamic description of the relation between pressure, temperature, entropy, and so forth. In principle, these thermodynamic quantities can be calculated from knowing the various interatomic forces (Schrödinger Equation). Practically, phenomenological equations based on "partial" theories and experiments have been used. We used the wide range semiempirical EOS for metals (Bushman *et al.*, 1993*a*, 1993*b*), which describes our experimental conditions properly. This EOS takes into account the elastic interaction of the crystal lattice, the anharmonic thermal vibration of the nuclei, the contribution of the thermal excitation of the electrons, and the effects of melting, evaporation, and ionization. In the high temperature limit, the equation of state has the asymptotic behavior of ideal fully ionized plasma consisting of electrons and nuclei.

Figure 5 displays isotherms (the pressure as a function of the ratio of the specific volume to the standard specific volume) for aluminum, calculated using the above EOS.

The spall strength, for each temperature, is the negative pressure as given at the minimum point of the isotherm. The temperature corresponding to each isotherm is indicated on each curve. The temperature upon spalling is the temperature on the release isentrope, following the shock loading. According to the EOS, the spall strength slightly decreases with increasing temperature, below the melting point (at zero pressure), and drops dramatically as the material melts. Such behavior was observed in experiments for several metals (Kanel *et al.*, 1993, 1996*a*).

The above theoretical spall strength as calculated from the EOS is expected to place an upper bound on measured spall strengths. Under conditions of dynamic loading, the fracture mode is a time-dependent process, resulting from growth of voids, cracks, or other "defects" in metals. This process includes three steps: nucleation, growth, and coalescence of voids or fractures (Grady, 1988; Bushman et al., 1993*a*, 1993*b*; Grady & Kipp, 1993). As a result, the spall strength value is not a material constant but a function of the strain rate in the unloading part of the incident shock pulse. The strain rate is related to the duration of the loading. In experiments using plate impact or high explosives, strain rates up to 10^5–10^6 s^{-1} are reached. With laser-induced shock loading, it is possible to reach ultrahigh strain rates, due to the short duration of the laser-induced pressure pulse. At strain rates up to 10^6 s^{-1}, the resistance to spall strength changes slowly with the strain rate. The spall strength in the above strain rate regime is about one order of magnitude

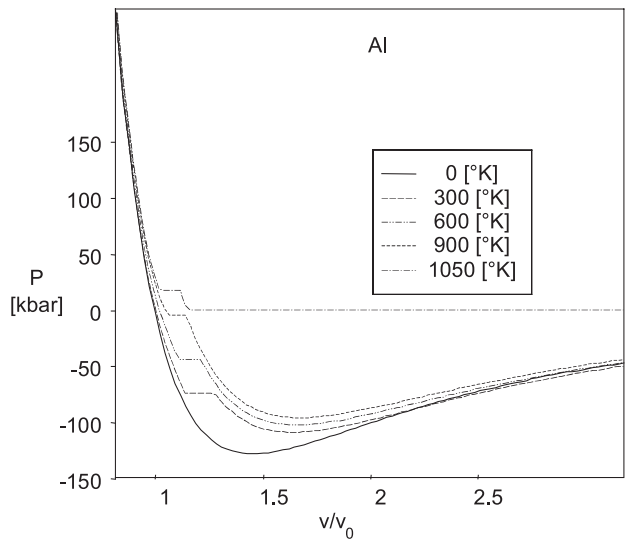

Fig. 5. Isotherms of Al, calculated with the wide-range semiempirical EOS.

https://doi.org/10.1017/S0263034602201123 Published online by Cambridge University Press

smaller than the EOS spall strength. This behavior is explained by initial flaws and cavities (ductile metals) or cracks (brittle metals) in the material, which grow and move under tension until the material between them undergoes local plastic flow and breaks, thus weakening the material. At higher strain rates, or shorter loading times, the initial flaws do not have time to move and coalesce and produce an observable spall, and the interatomic forces become more important. At these high strain rates ($>10^6$ s^{-1}), new cavities are formed spontaneously under tension, as a result of the material being in a metastable state (Kanel *et al.*, 1996*a*; Dekel *et al.*, 1998). These cavities grow and coalesce until their total volume is of the order of magnitude of the volume of the material at the spall area. The force needed to dislocate a single atom is given by the interatomic forces, but there is no demand that all the atoms be dislocated simultaneously. Therefore, at high strain rates, the strength is determined by both the interatomic forces and by growth and nucleation of cavities.

The results of our measurements are plotted in Figure 6 for aluminum and copper.

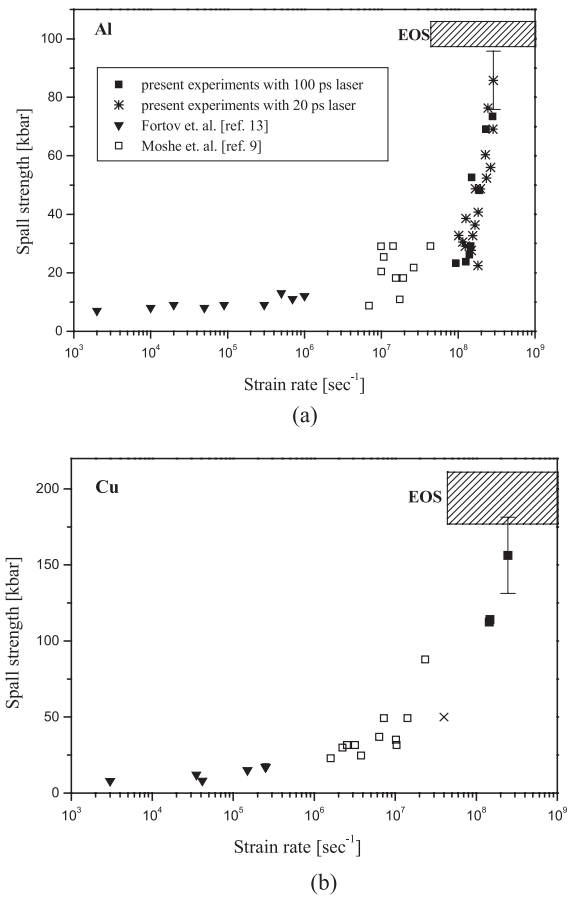

Fig. 6. (a) Spall strength as a function of the strain rate in Al. ■ Present experiments with 100 ps laser. *Present experiments with 20 ps laser. ▼Fortov *et al.*, 1991. □ Moshe *et al.*, 1998. (b) Spall strength as a function of the strain rate in Cu. ■ Present experiments. ▼ Kanel *et al.*, 1996*a*. × Paisley *et al.*, 1992. □ Moshe *et al.*, 1998.

We found out that the spall strength increased sharply as the strain rates increased beyond $5\cdot10^7$ s^{-1}. The spall strength values found at strain rates higher than 10^8 s^{-1} match the theoretical values calculated from the equation of state (Moshe *et al.*, 2000). For example, in aluminum we obtained a spall strength of 86 ± 10 kbar at a strain rate of $2 \pm 1\cdot10^8$ s^{-1}. The strength calculated from the equation of state in the temperature domain of our experiments is 101 to 108 kbar. For comparison the static strength of aluminum is 0.4 kbar and the dynamic strength at a strain rate of $1\cdot10^6$ s^{-1} is 12 kbar. In copper, we found a spall strength of 156 ± 20 kbar at a strain rate of $2 \pm 1\cdot10^8$ s^{-1}, while the equation of state predicts 172 to 211 kbar. The results for zinc and tin were similar (Moshe *et al.*, 1999). In other words, we have approached the maximum strength of materials and our spall pressures are the highest attainable. The accuracy of the free surface velocity is 5%; therefore the spall strengths measured in the experiments reported here are very close to the ultimate strength given by the EOS. These values are plotted in Figure 6 as the EOS spall strength, together with the spall pressures (for aluminum and copper), as function of the strain rate. Additional data measured in experiments using the impact of a projectile on a target (Fortov *et al.*, 1991; Kanel *et al.*, 1996*b*) and in experiments of nanosecond laser-induced shock waves (Paisley *et al.*, 1992; Moshe *et al.*, 1998) is also shown in Figure 6. Figure 7 shows our experimental data as in Figure 6a, but in a linear (nonlogarithmic) scale. It can be seen that the slope changes from $1\cdot10^{-7}$ kbar·s to $3\cdot10^{-7}$ kbar·s at strain rates of about $1\cdot10^8$ s^{-1}.

4. SUMMARY

A diagnostic system (ORVIS) was developed for continuos measurement of the free surface velocity of laser-shocked materials (without disturbing the process).

This system was used to measure the dynamic pressure for spall as a function of the strain rate in the range of $5\cdot10^6$–$5\cdot10^8$ s^{-1}. Measurements were carried out in

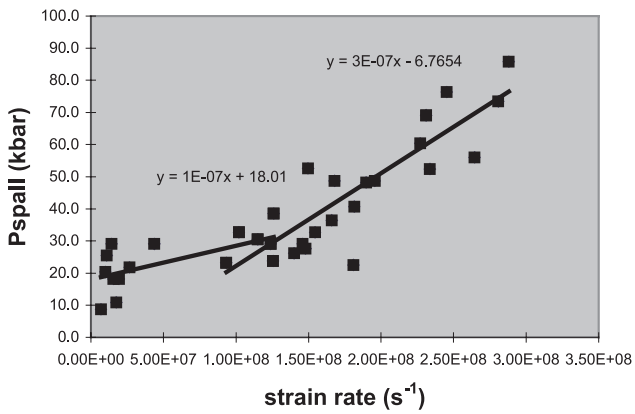

Fig. 7. The spall strength as a function of the strain rates—aluminum (nonlogarithmic scale).

https://doi.org/10.1017/S0263034602201123 Published online by Cambridge University Press

aluminum, copper, tin, zinc, and an amorphous material ($Fe_{80}B_{11}Si_9$).

The results show a sharp rise in the spall strength at the high strain rates when approaching the theoretical value predicted by the EOS of the materials at $5 \cdot 10^8$ s^{-1}. The results with the amorphous alloy prove that, at high strain rates, the material strength is determined mostly by the interatomic forces and less by initial flaws. A model describing the spall development at high strain rate fits the experimental results fairly well.

This research is unique in the field of dynamic strength of materials due to the measurements and analysis of the transition from phenomena dominated by macroscopic defects, flaws-governed phenomenon to a microscopic mechanism determined by atomic forces.

ACKNOWLEDGMENTS

The authors greatly acknowledge the contribution of the plasma group at SOREQ: Z. Henis, M. Werdiger, Y. Horovitz, S. Maman, and E. Dekel.

REFERENCES

Barker, L.M. & Schuler, K.W. (1974). Correction to the velocity-per-fringe relationship for the VISAR interferometer. *J. Appl. Phys*. **45**, 3692–3693.

Baumung, K. & Singer, J. (1995). *Physics of Intense Light Ion Beams and Production of High Energy Density in Matter*, Annual Report 1994, p. 88, Karlsruhe: Forschungzentrum Karlsruhe GmBH.

Bloomquist, D.D. & Sheffield, S.A. (1983). Optically recording interferometer for velocity measurements with subnanosecond resolution. *J. Appl. Phys*. **54**, 1717–1722.

Bushman, A.V., Kanel, G.I., Ni, A.L & Fortov V.E. (1993*a*). Fracture under pulsed loading. Spallings strength. In *Intense Dynamic Loading of Condensed Matter*, Ch. 5, pp. 74–99. London: Taylor & Francis.

Bushman, A.V., Kanel, G.I., Ni, A.L & Fortov V.E. (1993*b*). Generalized equations of state for metals. In *Intense Dynamic Loading of Condensed Matter*, Ch. 8, pp. 142–149. London: Taylor & Francis.

Dekel, E., Eliezer, S., Henis, Z., Moshe, E., Ludmirsky, A. & Goldberg, I.B. (1998). Spallation model for the high strain rates range. *J. Appl. Phys*. **84**, 4851–4858.

Eliaz, N., Moshe, E., Eliezer, S. & Eliezer, D. (2000). Hydrogen effects on the spall strength and fracture characteristics of amorphous Fe-Si-B alloy at very high strain rates. *Metall. Mater. Trans. A* **31A**, 1085–1093.

Fortov, V.E., Kostin, V.V. & Eliezer, S. (1991). Spallation of metals under laser irradiation. *J. Appl. Phys*. **70**, 4524–4531.

Grady, D.E. (1988). The spall strength of condensed matter. *J. Mech. Phys. Solids* **36**, 353–384.

Grady, D.E. & Kipp, M.E. (1993). Dynamic fracture and fragmentation. In *High Pressure Shock Compression of Solids*, Ch. 8, pp. 265–322. New York: Springer.

Kanel, G.I., Razorenov, S.V., Bogatch, A., Utkin, A.V., Fortov, V.E. & Grady, D.E. (1996*a*). Spall fructure properties of aluminum and magnesium at high temperatures. *J. Appl. Phys*. **79**, 8310–8317.

Kanel, G.I., Razorenov, S.V., Utkin, A.V., Fortov, V.E., Baumung, K., Karow, K.U., Rush, D. & Licht, V. (1993). Spall strength of molybdenum single crystals. *J. Appl. Phys*. **74**, 7162–7165.

Kanel, G.I., Razorenov, S.V. & Utkin, A.V. (1996*b*). Spallation in solids under shock-wave loading: Analysis of dynamic flow methodology of measurements and constitutive factors. In *High-Pressure Shock Compression of Solids* II, pp. 1–24 (Davison, L., Grady, D.E. & Shahinpoor, M., Eds.). New York: Springer-Verlag.

Moshe, E., Dekel, E., Henis, Z. & Eliezer, S. (1996). Development of an optically recording velocity interferometer system for laser induced shock waves measurements. *Appl. Phys. Lett*. **69**, 1379–1381.

Moshe, E., Eliezer, S., Dekel, E., Henis, Z., Ludmirsky, A., Goldberg, I.B. & Eliezer, D. (1999). Measurements of laser driven spallation in tin and zinc using an optically recording velocity interferometer system. *J. Appl. Phys*. **86**, 4242–4248.

Moshe, E., Eliezer, S., Dekel, E., Ludmirsky, A., Henis, Z., Werdiger, M., Goldberg, I.B., Eliaz, N. & Eliezer, D. (1998). An increase of the spall strength in aluminum, copper and Metglas at strain rates larger than 10^7 s^{-1}. *J. Appl. Phys*. **83**, 4004–4011.

Moshe, E., Eliezer, S., Henis, Z., Werdiger, M., Dekel, E., Horovitz, Y., Maman, S., Goldberg, I.B. & Eliezer, D. (2000). Experimental measurements of the strength of metals approaching the theoretical limit predicted by the equation of state. *Appl. Phys. Lett*. **76**, 1555–1557.

Paisley, D.L., Warmes, R.H. & Kopp, R.A. (1992). Laser driven flat plate impacts to 100 Gpa with sub-nanosecond pulse duration and resolution for material property studies. In *Shock compression of Condensed Matter 1991*, pp. 825–828. New York: Elsevier Science.